Chemical Engineering Science 100 (2013) 402–412

Contents lists available at SciVerse ScienceDirect

Chemical Engineering Science

journal homepage: www.elsevier.com/locate/ces

Discrete axial motion of a radioactive tracer reconstructed from the response of axially aligned detectors: Application to the analysis of a bubble column dynamics

Gabriel L. Salierno [a], Mauricio Maestri [a], Stella Piovano [a], Miryan Cassanello [a,*], María Angélica Cardona [b,c], Daniel Hojman [b], Héctor Somacal [b,c]

[a] PINMATE, Departamento de Industrias, FCEyN, Universidad de Buenos Aires, Intendente Güiraldes 2620, C1428BGA Buenos Aires, Argentina
[b] Departamento de Física, Comisión Nacional de Energía Atómica (CNEA), Buenos Aires, Argentina
[c] ECyT, Universidad Nacional de San Martín, San Martín, Argentina

HIGHLIGHTS

- Axial trajectories of a moving tracer can be got with axially aligned detectors.
- Persistent tracer axial motions provides information on the liquid velocity.
- Liquid mixing and recirculation times can be estimated from the tracer trajectory.
- Gas holdup axial profiles from the tracking agree with those obtained by scanning.
- The influence of liquid viscosity on the tracer trajectories is studied.

ARTICLE INFO

Article history:
Received 5 September 2012
Received in revised form
6 March 2013
Accepted 17 March 2013
Available online 29 March 2013

Keywords:
Axially aligned detectors
Radioactive tracers
Bubble column hydrodynamics
Mixing times
Gas holdup profiles
Flow regimes

ABSTRACT

The feasibility of extracting relevant dynamic information of a bubble column from the approximate reconstruction of a radioactive tracer axial trajectory using a set of axially aligned detectors (AAD) is explored. The experimental procedure involves scanning simultaneously different column heights with scintillation detectors, located vertically aligned beside the examined vessel, while a neutrally buoyant radioactive tracer particle is freely moving inside. The reconstruction considers that the detectors located closer in axial coordinate to the tracer are the ones which record the largest number of counts. Based on this assumption, time series of the approximate tracer axial coordinate are obtained with a maximum resolution of $2N-1$ (N: number of detectors used). Compared to the powerful radioactive particle tracking (RPT) technique, although the information extracted is more limited, the present experimental procedure has the advantage of not requiring a calibration stage, which is rather cumbersome to implement at industrial scale and prevents RPT massive use for troubleshooting. Part of the information extracted from the analysis of tracer axial trajectories in RPT can also be inferred from the discrete tracer axial trajectories obtained with this methodology. Therefore, tracer fast axial velocity distributions, liquid axial mixing time and liquid holdup axial profiles are estimated from the reconstructed axial trajectories and related to the operating conditions, for experiments with water and non-Newtonian aqueous solutions of carboxymethyl cellulose (CMC).

1. Introduction

Bubble columns are gas–liquid contactors which are largely employed, particularly because of their low operating and maintenance costs, absence of moving parts and little floor space requirements. In addition, high transfer rates, large interfacial areas, and the possibility of operation with solids without serious erosion or plugging problems promote the use of these contactors in quite diverse fields. Therefore, many applications of these units can be found in the chemical, petrochemical, pharmaceutical, food and environmental industries (Kantarci et al., 2005).

Despite their simple construction and operation, bubble columns can be rather difficult to design and scale-up due to their extremely complex hydrodynamics, which has been, and still is, extensively studied. Non-invasive methods are required to capture

* Corresponding author. Tel.: +54 11 45763383; fax: +54 11 45763366.
E-mail addresses: cassanello_m@yahoo.com.ar, miryan@di.fcen.uba.ar (M. Cassanello).

0009-2509/$ - see front matter © 2013 Elsevier Ltd. All rights reserved.
http://dx.doi.org/10.1016/j.ces.2013.03.029

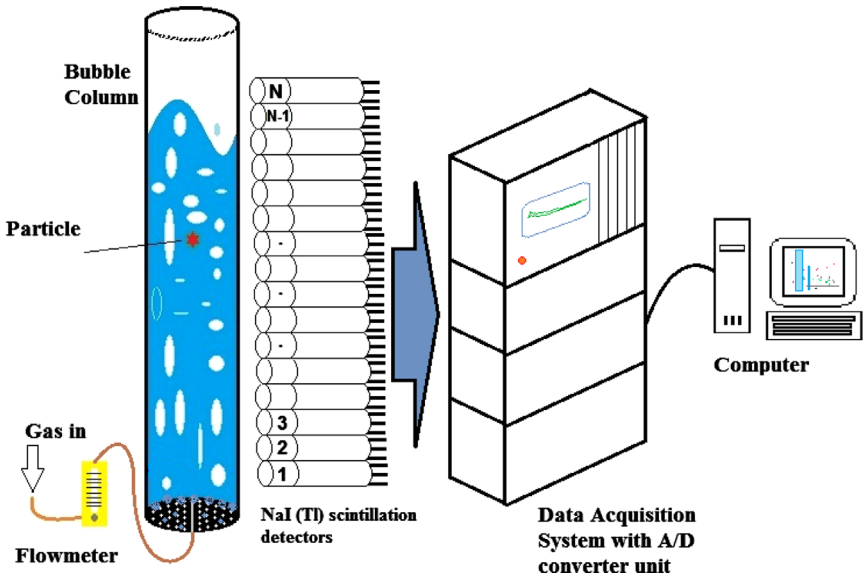

Fig. 1. Schematics of the installation.

the undisturbed dynamics of these units and, due to the inherently opaque nature of the multiphase flows, radioactive methods have proved to be very appropriate (Chaouki et al., 1997; Dudukovic, 2002; Heindel, 2011). Among them, radioactive particle tracking (RPT) is a powerful technique used to thoroughly examine the dynamics of condensed phases (fluidized solid or liquid) in opaque media. RPT has been applied to extract features of many different multiphase vessels representing multiphase reactors (Dudukovic, 2002). Part of the information arising from RPT is related to the analysis of the tracer axial trajectory, and especially when the tracer undergoes fast ascending paths (Larachi et al., 1996; Cassanello et al., 1996, 2001). Even if RPT provides a complete panorama of the examined vessel, it is rather complicated to implement in actual industrial installations mainly due to the required calibration stage under actual operating conditions. In this context, this work has the aim of determining the approximate axial path of a radioactive tracer freely moving within a bubble column from the combined response of axially aligned scintillation detectors (AAD), avoiding the demanding calibration required for RPT. Moreover, the feasibility of inferring information of the underlying dynamics in bubble columns from the reconstructed tracer axial path is discussed.

2. Experimental

The experimental facility includes an acrylic cylindrical vertical bubble column (1.2 m height and 0.1 m inner diameter) provided with a perforated plate gas distributor, mounted onto a structure jointly to an array of 8 or 11 axially aligned $2'' \times 2''$ NaI(Tl) scintillation detectors, as illustrated in the scheme shown in Fig. 1. Each scintillation detector is provided with the corresponding photomultiplier and the electronics required for determining the number of photons with energies close to the photopeak of the characteristic γ-rays of the radioisotope used for the experiments. Two configurations of detectors have been tested. First, 8 detectors have been located separated 0.1 m in-between and the first one was 0.1 m above the distributor line. The complete array surpasses the emulsion height. Based on results obtained with this configuration, it was observed that the first detector should be closer to the distributor line to have equally spaced compartments in the discretization. Also, it was decided to increase the number of detectors to improve the resolution. The error in tracer position can be estimated in half the distance between detectors; hence, the more the number of detectors that can be accommodated linearly aligned besides the column to completely cover the emulsion height at the highest gas velocity used, the better the resolution. Then, the second configuration tested involved 11 detectors separated 0.06 m in-between and the first one was located 0.03 m above the distributor line. Smaller detectors would lead to a better granularity provided the tracer intensity is strong enough for the detectors to count a recordable number of photons. Nevertheless, smaller detectors imply smaller intrinsic efficiencies. To improve the granularity maintaining the efficiency, special small detectors could be used: (a) long axis NaI detectors with small diameter or (b) $1'' \times 1''$ $LaBr_3$ detectors. Both solutions will produce a very important increase in the cost of the system. Whatever the detectors used, they should be of similar size and efficiency.

Table 1
Rheological characteristics of the model liquids employed.

Liquid	k (mPa s^n)[a]	n[a]
Water	1	1
CMC 0.75% w/w	140	0.88
CMC 1.1% w/w	510	0.77
CMC 1.5% w/w	902	0.74
CMC 2.0% w/w	4122	0.66

[a] Parameters k and n correspond to the Ostwald–de Waele relation: $\tau = k(\dot{\gamma})^n$.

Tap water and non-Newtonian aqueous solutions of carboxymethyl cellulose sodium salt (0.75–2% w/w Fluka high viscosity) were used in batch as model liquids. Rheological characteristics of the liquids used have been determined with a Brookfield viscometer and described by the Ostwald–de-Waele relation as expressed in Eq. (1), where τ is the shear stress, $\dot{\gamma}$, the shear rate, k is a consistency index and n, an index of flow behavior (Bird et al., 2006). Best fitted parameters, k and n, corresponding to the fluids used are given in Table 1.

$$\tau = k(\dot{\gamma})^n \tag{1}$$

The gas phase was air, fed from a compressor. The liquid level at rest was kept in the range 0.5–0.6 m and the maximum emulsion height was generally lower than 0.7 m. Different gas velocities within the range 0.011–0.125 m/s were tested for each of the model liquids employed. The distributor is a gas–liquid distributor

with the liquid holes blocked, since liquid was in batch mode. It was built following the guidelines suggested by Lee et al. (2001); the gas enters the column through 56 holes of 0.001 m, representing 0.56% of the column section. Details of the distributor design can be found in Fraguío (2010).

The tracers used were prepared by encapsulating tiny pieces of gold in polyethylene beads (of approximately 0.002 m diameter), which were scraped to turn them neutrally buoyant in the model liquids used. After reaching the desired density, tracers were activated prior to each experiment by neutron bombardment in the RA1 reactor of CNEA to get ^{198}Au ($E\gamma$=412 keV, $T_{1/2}$=2.7 d) with activities of about 80 μCi. Experiments consisted in following the motion of the tracer with the AAD array for an hour while it was freely moving within the column at each of the explored experimental conditions. Gamma counting sampling period was set to 10 ms; thus, experimental time series for each run have 360,000 points. It should be mentioned that the results did not change significantly when using the complete time series or half of it for the analysis carried out, indicating that the number of events was appropriate for getting the mean information that was extracted. However, longer tracking would always be preferable to have more reliable statistics. The tracers used are large to track small high frequency eddies. However, eddies responsible for fluctuations in the small scale cannot be captured with the coarse reconstruction methodology. Only, low frequency high energy containing vortices, largely responsible of the gross liquid circulation can be properly captured with this method.

Apart from the experiments with the tracer freely moving within the vessel, scanning experiments were performed by locating a 2 mCi ^{241}Am ($E\gamma$=60 keV, $T_{1/2}$=432.7 yr) sealed source located diametrically opposite to each AAD, for determining the chordal liquid holdup at different column heights at the same explored experimental conditions following the standard procedure (Chaouki et al., 1997).

3. Axial trajectory reconstruction procedure

When the tracer is freely moving within the column, the number of counts determined by each AAD depends on the tracer activity, the detector dead time, the media attenuation and mainly on the distance separating the detector crystal from the tracer instantaneous position. Due to the AADs arrangement and column geometry, it is expected that the detector closest to the tracer in axial coordinate will measure the maximum number of counts provided the counting period is sufficiently short. This assumption would be strictly valid for detectors having the same size, efficiency and dead time, and with constant media attenuation. Detectors used in this case have all similar size and efficiency and the dead time is less than the microsecond. Variations along the column are only related to differences in the mean attenuation arising from differences in gas holdup. To verify if the assumption holds under a normal experimental condition, the MonteCarlo methodology developed by Larachi et al. (1994) for radioactive particle tracking (RPT) tracer path reconstruction was applied to simulate the intensities that will be measured by each detector when the tracer is located at many positions all over the column. For performing the simulation, a manual calibration as the one usually required for a RPT experiment was carried out by locating the tracer at 150 known positions within the column while recording the response of the detectors. With this data, the Monte Carlo model parameters (detector efficiency, media attenuation and detector dead time) have been fitted for each detector. As expected, dead time was less than the microsecond and efficiency was similar for all the detectors, only small differences in the mean attenuation of the media were apparent. Further details on the calibration and reconstruction methodology used for RPT experiments in this facility can be found in Fraguío (2010). The calibration was done at a high gas velocity, for which the variations in media attenuation along the column could be significant due to variations in gas holdup.

Fig. 2a illustrates the number of counts that would be recorded by 8 AADs as estimated with the simulation while the tracer is located at 81,000 internal positions within the bubble column. Black line on top indicates the axial location of each detector crystal. As observed, the number of counts peaks when the tracer axial position is located close to the detector axial position. Fig. 2b shows the counts of the eight considered detectors, normalized with the maximum number of counts recorded at a given position. When the tracer is located close in axial position to a given

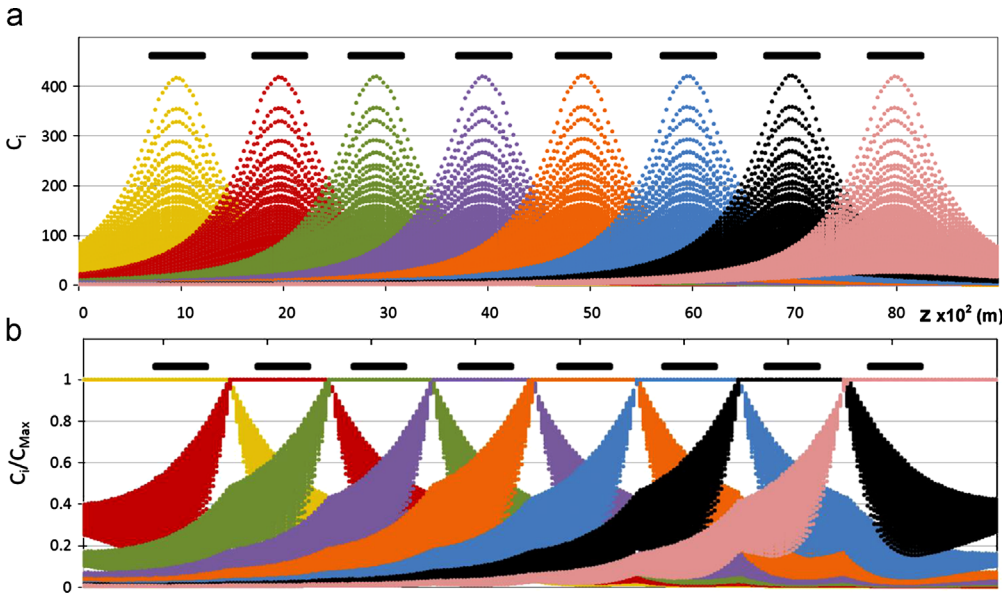

Fig. 2. Number of counts that would be measured by 8 AADs estimated by simulation using the model developed by Larachi et al. (1994) when (a) the tracer is located at 81,000 positions within the column and (b) the same normalized with the counts of the detector that measures the maximum number for each position. Black line on top indicates axial position spanned by each detector crystal.

detector, the normalized measure of that detector is always unitary, being very low for all the other detectors. When the tracer is in between two detectors in the axial coordinate, both involved detectors have fractional values significantly larger than the others. Hence, from the combined response of the AADs measured when the tracer is left in free motion within the vessel, its axial position is assigned to the center of the detector that measures the maximum number of counts during a given counting period if all the others measure less than a given percentage of the maximum number of counts, imposed as a threshold. When the normalized number of counts of a second detector is also larger than the threshold, the axial position of the tracer is assigned to the middle point between the two detectors with normalized number of counts that surpasses the threshold. In this way, time series of the approximate tracer axial coordinate, with a maximum granularity of $2N-1$ (N: number of detectors used), are obtained without the requirement of a calibration stage.

Therefore, the reconstruction procedure is to search, at each instant, the detector which measures the maximum number of counts and to normalize all the signals with respect to that value. Then, a threshold is considered to decide if the tracer axial location is assigned to the level of the detector that measures the maximum number of counts or in the middle position between this detector and the second one in the number of counts recorded; from the simulation, the threshold was set in 75% (i.e., if the number of counts measured by the second detector is more than 75% of the maximum, the position is assigned to the middle in-between detectors).

The reconstruction procedure leads to approximate axial positions; the uncertainty can be estimated in half the distance

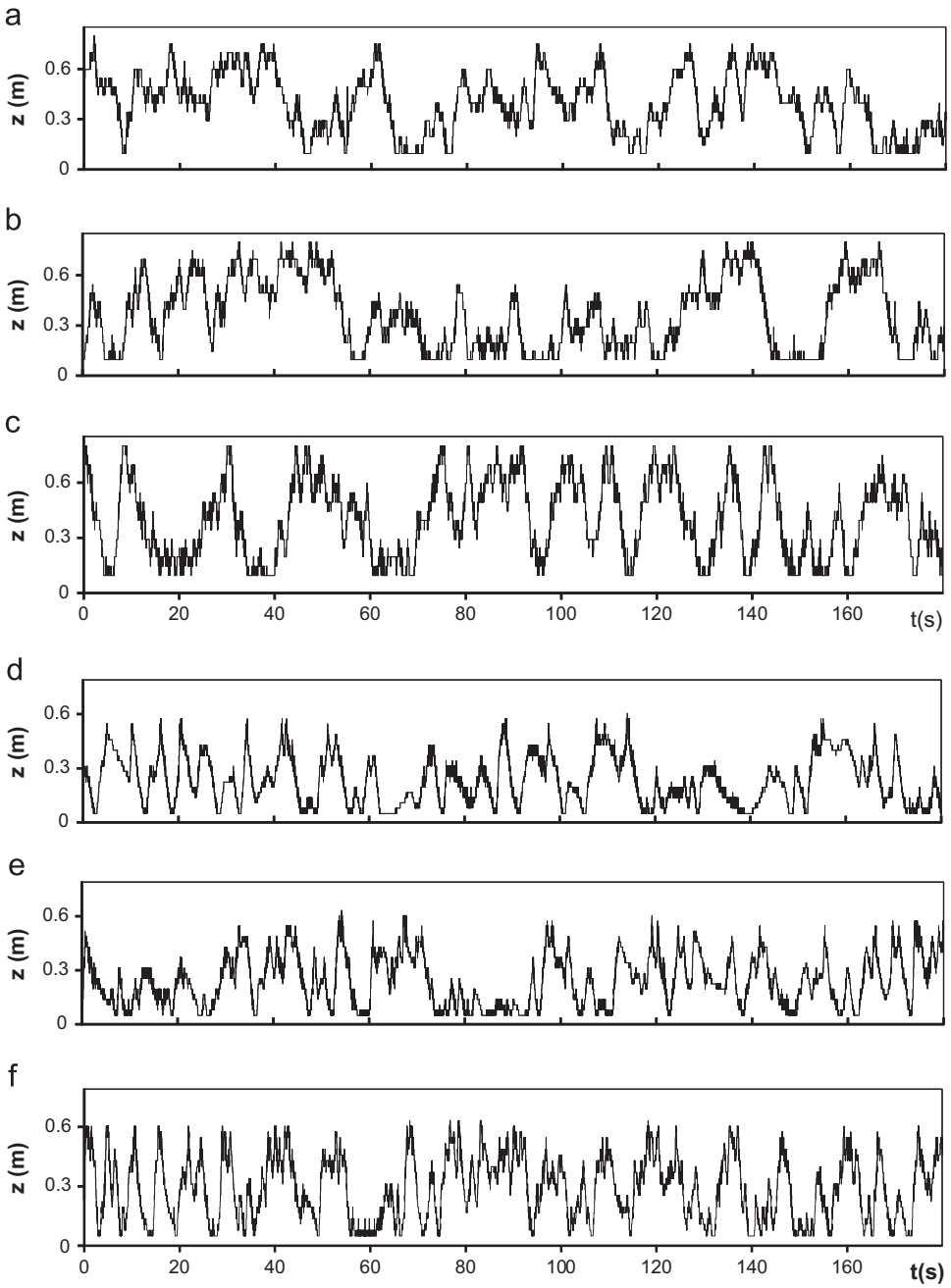

Fig. 3. Typical radioactive tracer axial coordinate time series reconstructed from the combined response of the AADs arrays: (a)–(c) water with 8 AADs; (d)–(f) aqueous solution of CMC (1.1% w/w) with 11 AADs. Gas velocity indicated in the legend. (a) ug=0.032m/s, (b) ug=0.064m/s, (c) ug=0.106m/s, (d) ug=0.032m/s, (e) ug=0.064m/s and (f) ug=0.106m/s.

between detectors. For this reason, instantaneous velocities calculated by differentiating successive positions have too large errors and only velocities leading to long motions of the tracer can be determined reliably from the tracking.

4. Results

The reconstructed discrete axial trajectories of the tracer during 3 min for representative experiments carried out with water and with an aqueous solution of 1.1% w/w CMC, using 8 and 11 detectors, respectively, are shown in Fig. 3, for different gas velocities. As observed in the figure, the trace resolution certainly improves with the number of detectors.

The tracer explores axially the whole column many times during a 3 min track; it should be kept in mind that the tracer motion represents the liquid axial motion of low frequency since it is neutrally buoyant but of relatively large size, preventing the correct tracking of small eddies. As the gas velocity increases, the motion becomes more violent, appearing frequently fast ascending and descending paths crossing long distances in very short periods of time. The long fast motions of the tracer are likely to be related to the passage of large bubbles, when the tracer travels the whole column, and when the excursions are of the order of 1–3 column sizes, by large vortical structures imposed by the gas circulation (Chen et al., 1994; Larachi et al., 1996; Joshi et al., 2002; Mudde, 2005).

5. Tracer velocity distributions

The time series of the tracer axial trajectory frequently show fast ascending and descending paths. Fast tracer upward motions observed in RPT experiments have been related to the existence of big bubbles and bubbles' bursts in bubble columns and three phase fluidized beds (Larachi et al., 1996; Cassanello et al., 2001). Larachi et al. (1996) interpreted the appearance of steeped ascensions crossing long axial extensions within the column in short times at almost constant velocities as related to the tracer being entrapped in the wake of fast ascending bubbles. Fast ascending paths are not necessarily related to the tracer entrapped in a bubble wake unless the motion travels the whole column in very short time; more frequently they would arise from the tracer within the large vortical structures that appear in the column imposed by the swirling motion of the bubble stream traveling preferentially around the column center (Chen et al., 1994; Joshi et al., 2002; Mudde, 2005). Descending paths have also been used to get information of the underlying dynamics in multiphase systems (Cassanello et al., 2001; Bhusarapu et al., 2007), and they also reflect the motion of the tracer within large vortical structures. Instantaneous velocities calculated by differentiating successive tracer positions would have too much error arising from the coarse reconstruction of the trajectory. However, if only the long persistent paths lasting more than 0.2 s are considered, the error is considerably lower. The velocity can be calculated either by the distance traveled by the tracer divided by the elapsed time during the ascension or from the slope of the motion calculated by linear estimation as suggested by Fraguío (2010).

Therefore, steeped and persistent ascending tracer paths found in the experiments at different gas velocities have been extracted from the tracking and the distributions of the neutrally buoyant tracer upward velocities have been calculated. In addition, persistent descending tracer paths, which have been reported to occur generally closer to the vessel wall in bubble columns (Cassanello et al., 2001), have also been analyzed to determine the corresponding velocity distribution.

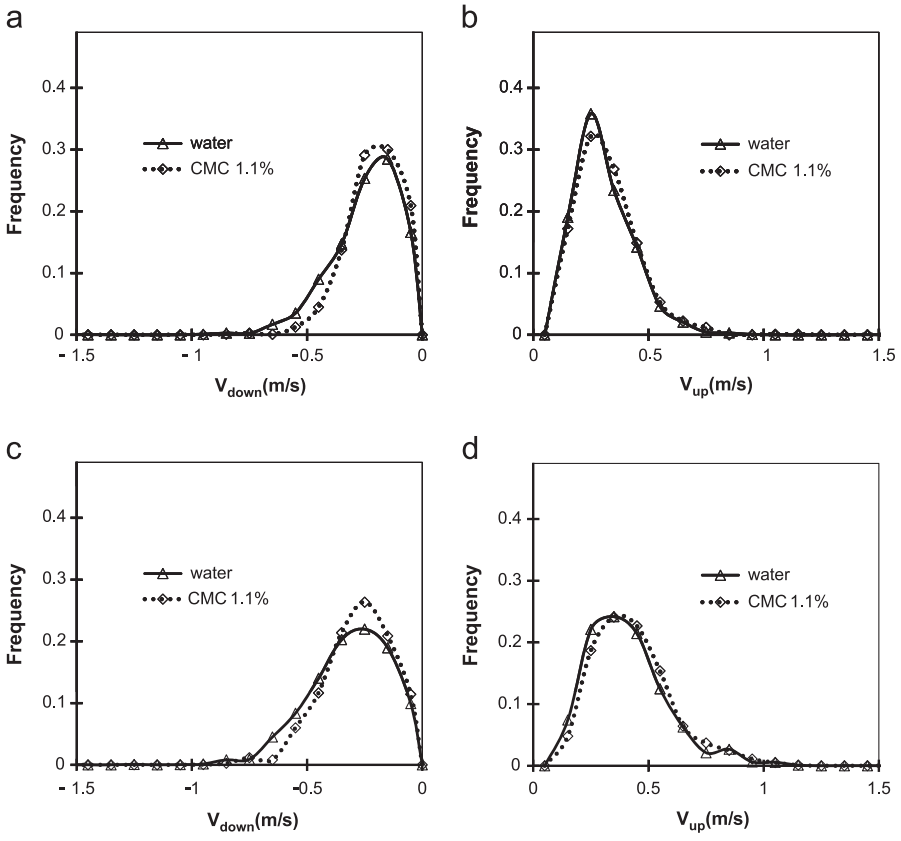

Fig. 4. Tracer axial upwards and downwards velocity distributions for experiments at two representative gas velocities and liquids of different viscosity. (a) ug=0.032 m/s - descending, (b) ug=0.032 m/s - ascending, (c) ug=0.106 m/s - descending and (d) ug=0.106 m/s - ascending.

Fig. 4 shows the distribution of tracer velocities calculated from ascending paths longer than 15% of the total gas–liquid expansion, for two gas velocities and liquids of different viscosities. In addition, the distribution of persistent downwards velocities for more than 5% of the emulsion expansion are also shown in the figure.

Tracer upward and downward axial velocity distributions are broader for higher gas velocities for all the liquids. As the liquid viscosity increases, the upward velocity distribution becomes slightly broader, while the downward velocity distribution shows the opposite behavior. Consequently, the tracer mean axial upward velocity increases as the gas velocity and the liquid viscosity increase. The influence of the liquid viscosity is likely related to the increase in bubble coalescence for more viscous liquids, leading to larger bubbles. On the contrary, the tracer mean descending velocity decreases as the gas velocity decreases and as the liquid viscosity increases. For downward motion, the influence of liquid viscosity probably arises from the larger friction of the liquid in the wall, region where the persistent descending paths are generally encountered.

Fig. 5a summarizes the influence of gas velocity and liquid viscosity (as a parameter) on the mean tracer upward axial velocities when it is moving with an almost constant velocity for persistent tracer paths, longer than 15% of the total emulsion expansion. Fig. 5b illustrates the influence of gas velocity and liquid viscosity on descending tracer velocities. The module of the axial velocity (either upward or downward) increases as the gas velocity increase, and moderately depends on the liquid viscosity, resulting in higher upwards velocities and lower downward velocities for more viscous liquids.

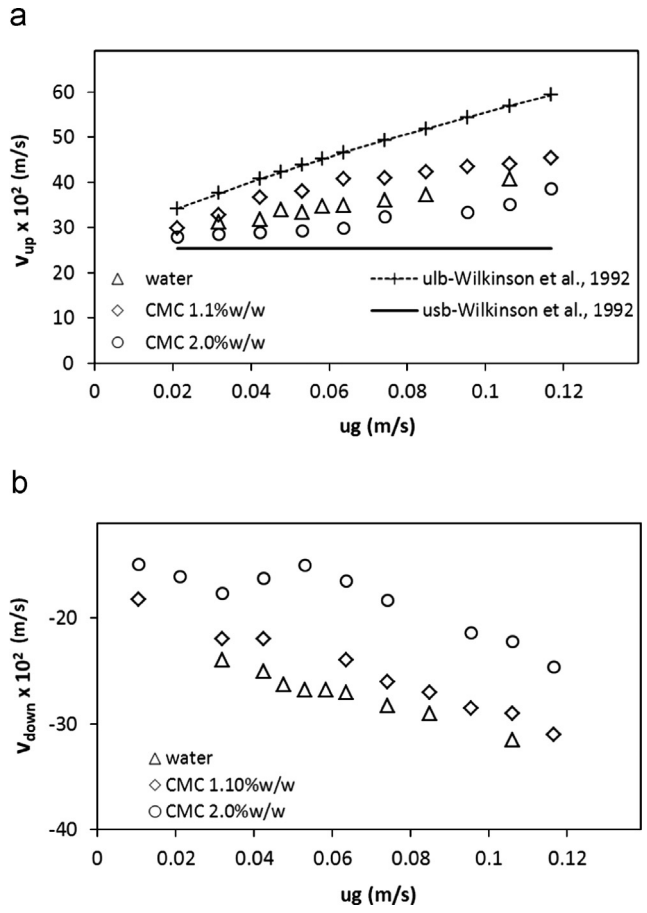

Fig. 5. Effect of the gas velocity and liquid viscosity on the mean tracer axial fast upwards (a) and downwards (b) velocities.

The small and large bubbles velocities, estimated by the correlation of Wilkinson et al. (1992) for water, are included in Fig. 5a for comparison. The tracer mean axial velocity approximately follows the trend of large bubbles velocities predicted by Wilkinson et al. (1992) with lower absolute values. The velocities of the highest viscosity liquid (2%w/w CMC aqueous solution) do not follow the trend. For this liquid, large bubbles covering the whole column diameter are apparent, indicating the inception of slug flow, which probably alters the macroscopic liquid recirculation.

Groen et al. (1996) have measured liquid velocities in a 3D bubble column with laser Doppler anemometry (LDA) and evidenced that the liquid motion is an outcome of the passage of dominant coherent structures with sizes of the order of the column diameter and having typical velocities. Several conditions, particularly those corresponding to high gas velocities, led to more than one typical velocity. In this case, only fast liquid velocities are captured, thus liquid velocities close to zero arising from high frequency fluctuations are not apparent in the distributions; then, the mean velocities calculated in the present work would be comparable to the largest typical velocities measured by Groen et al. (1996). The largest typical velocities reported by Groen et al. (1996) in a bubble column of 0.15 m with water as model liquid were 0.29 m/s and 0.32 m/s, respectively, for gas velocities of 0.032 m/s and 0.057 m/s. In the present work, the mean velocities calculated from fast ascending tracer paths for gas velocities of 0.032 m/s and 0.058 m/s are, respectively, 0.31 m/s and 0.35 m/s. The obtained mean liquid upward velocity for an experiment at 0.048 m/s (i.e., 0.33 m/s) also compares reasonably well with the mode of the distribution of liquid upwards velocities determined by Cassanello et al. (2001) for a bubble column of 0.16 m at a gas velocity of 0.05 m/s from RPT experiments.

6. Mixing time

The time required to attain axial complete liquid mixing from local injections at different sections in the bubble column can also be determined from the axial trajectory of a freely moving neutrally buoyant tracer, representing the liquid phase. Since the column height is quite larger than the column radius, complete mixing in the axial coordinate will generally be attained after section mixing and it could be a good estimation of the liquid mixing time. Injections from given axial positions can be reconstructed from the trajectory of a single tracer if the tracking is sufficiently long, taking trajectories of the tracer starting at the same column height at different times (Cassanello et al., 1996). The trajectories should not overlap in time to avoid correlations. Fig. 6 illustrates the axial coordinate evolution of 10 representative tracer trajectories starting from given axial locations along the column, for an experiment with 1.1% w/w CMC aqueous solution and 0.053 m/s gas velocity.

The followed trajectories (representing different elements injected at a given position) are close in time during the first 0.5 s whatever the injection region, and start to diverge as the time passes indicating that different elements are going to different regions in the column. From the figure, it also appears to be injection locations from which it is more difficult to attain mixing, particularly close to the column limits. These delays are likely related to the vortices that are generally present in bubble columns close to the gas entrance region (Devanathan et al., 1990; Groen et al., 1996; Degaleesan et al., 2001), and to interactions with bubbles bursts and eruptions in the column disengagement region that would keep the tracer and liquid elements fluctuating before reentering the gross macroscopic liquid recirculation imposed by the gas flow.

A situation of complete mixing would be attained when the probability of finding the elements "released" at the injection point is the same all over the column. Considering that each followed trajectory represents a different liquid element, this condition can be expressed as having equal fraction of released elements at different column regions. If the column is divided into N regions for the analysis, the most uniform distribution implies probabilities of $1/N$ for each region. The Shannon entropy, H, as defined in Eq. (2), is generally used to characterize the uniformity of a distribution (Shannon, 1948; Cover and Thomas, 1991).

$$H = -\sum_{j=1}^{N} \left[p_j \ \ln(p_j) \right] \tag{2}$$

where N is the number of bins in the histogram, and p_j is the probability of bin j. The Shannon entropy will have its maximum value when all the bins have the same probability; i.e., $p_j = 1/N$, for $j = 1,\ldots,N$ leading to $H_{max} = \ln(N)$. Therefore, to determine the condition of complete mixing, the statistics $\Omega(t)$ has been defined relating the Shannon entropy of the measured distribution for a given instant, to the maximum value that it can attain for the number of bins considered, as expressed by

$$\Omega(t) = \frac{H(t)}{H_{max}} = -\frac{\sum_{j=1}^{N} [p_j(t) \ \ln(p_j(t))]}{\ln(N)} \tag{3}$$

where $p_j(t)$ is calculated as the fraction of released elements found within region j at time t after the injection. Parameter $\Omega(t)$ can hardly reach the value of 1 since the liquid distribution along the column is not totally uniform, arising from variations in liquid holdup; hence, the criterion used to determine complete mixing is to consider the time required to reach the asymptotic maximum value of $\Omega(t)$. Typical time evolutions of the defined parameter for the same experiment used for illustration in Fig. 6 are shown in Fig. 7a–f. For getting the time required to accomplish complete mixing, whatever the injection point in the column, all the curves are represented together and the characteristic mixing time for a given condition arises from the convergence of all the curves. As examples, the convergence of the curves for the aqueous solution of CMC 1.1% w/w and for water are shown in Fig. 7g and h. It is observed that the curves converge more rapidly in the viscous solution mainly because the injections close to the gas distributor require less time to disperse.

To assert the influence of injection point on the time required for reaching the asymptotic value of $\Omega(t)$, the median of the computed values from the injection time to time t is compared to the median of $\Omega(t)$ during the whole trajectory. Representative mixing times estimated from injections at different columns heights are shown in Fig. 8 for experiments carried out with the aqueous solutions of 1.1% w/w CMC at different gas velocities. The mixing times evaluated from injections close to the boundaries and in the region corresponding to the vortex above the gas distributor are generally larger than those at mid-column heights. In the entrance region, the influence is more marked for high gas velocities, which induce more vigorous entrance vortices. In the upper region, apart from the effect of bubble eruptions, the increase in mixing time is related to the moving boundary that occasions fewer trajectories starting from this region. For this reason, injection points were considered only from 10% to 90% of the total emulsion expansion to determine the convergence of curves for estimating the mixing time for the whole column.

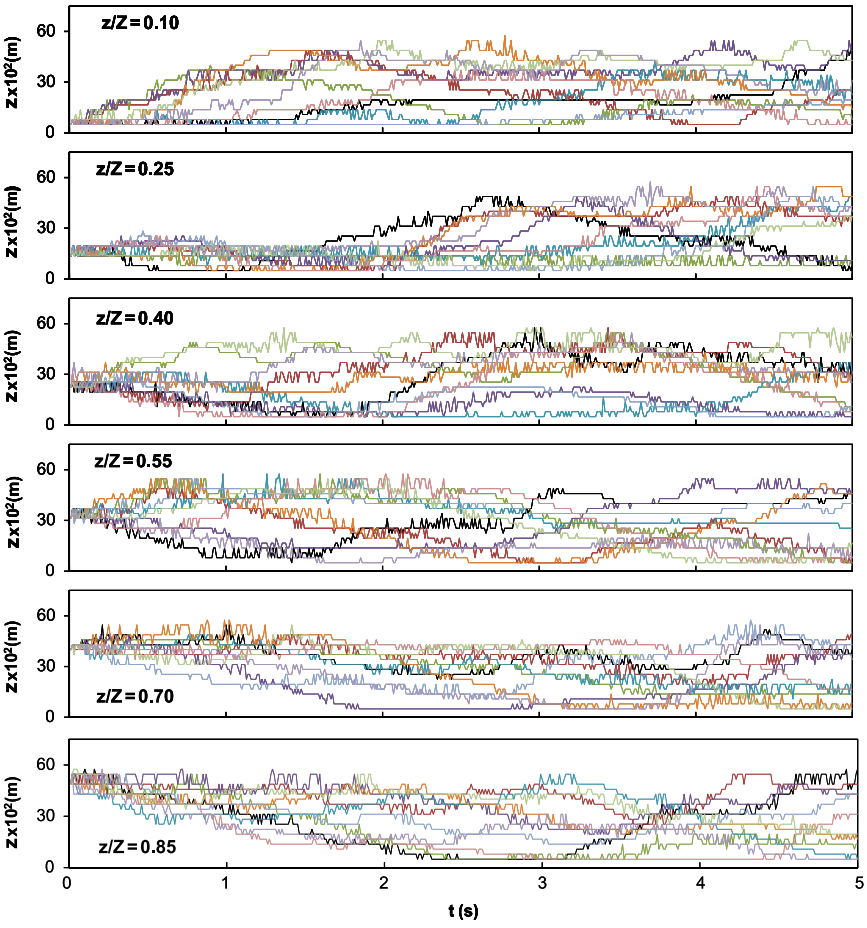

Fig. 6. Representative tracer axial trajectories during the 5 s after crossing given heights in the column at different times. The crossing height, referred to the total emulsion height, is indicated in the legend. Liquid: aqueous solution of CMC (1.1% w/w). Gas velocity = 0.053 m/s.

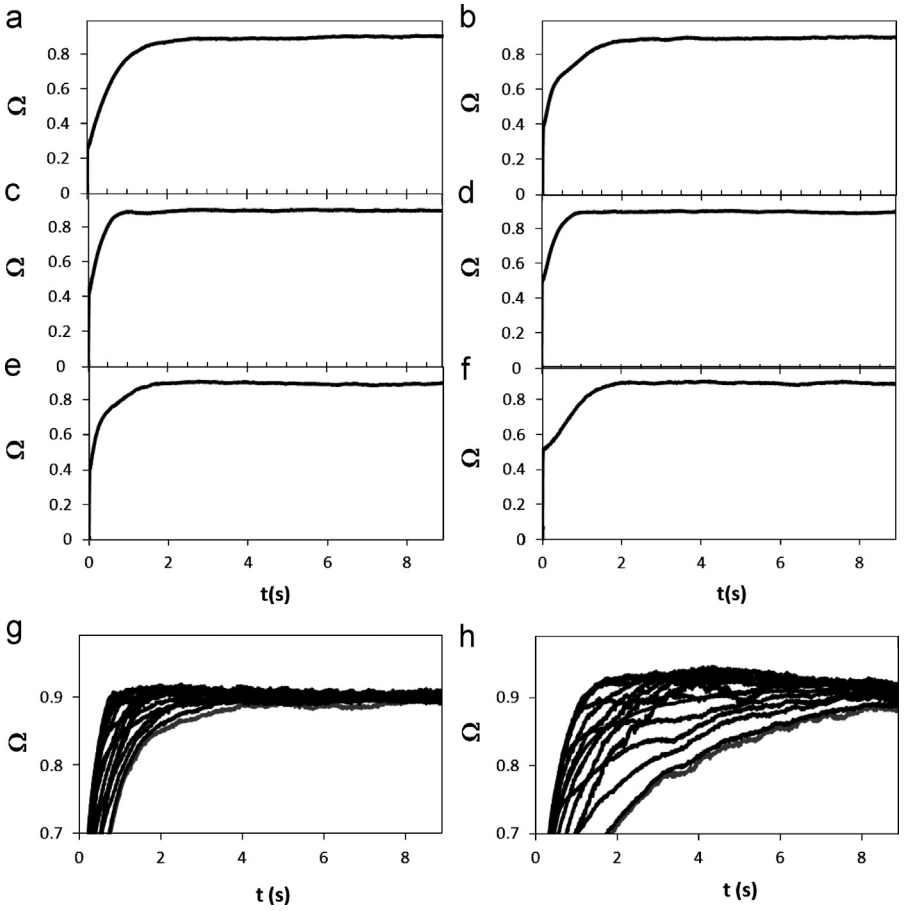

Fig. 7. Time evolution of the parameter defined in Eq. (3) for the same conditions and injection axial locations shown in Fig. 6(a)–(f). Convergence of the curves from different injection points for: an aqueous solution of CMC 1.1% w/w (g) and water (h).Gas velocity = 0.053 m/s. (a) z/H =0.1, (b) z/H = 0.2, (c) z/H = 0.4, (d) z/H = 0.6, (e) z/H = 0.8, (f) z/H = 0.9, (g) convergence from injections among z/H = 0.1 to 0.9 CMC 1.1% w/w and (h) convergence from injections among z/H = 0.1 to 0.9 water.

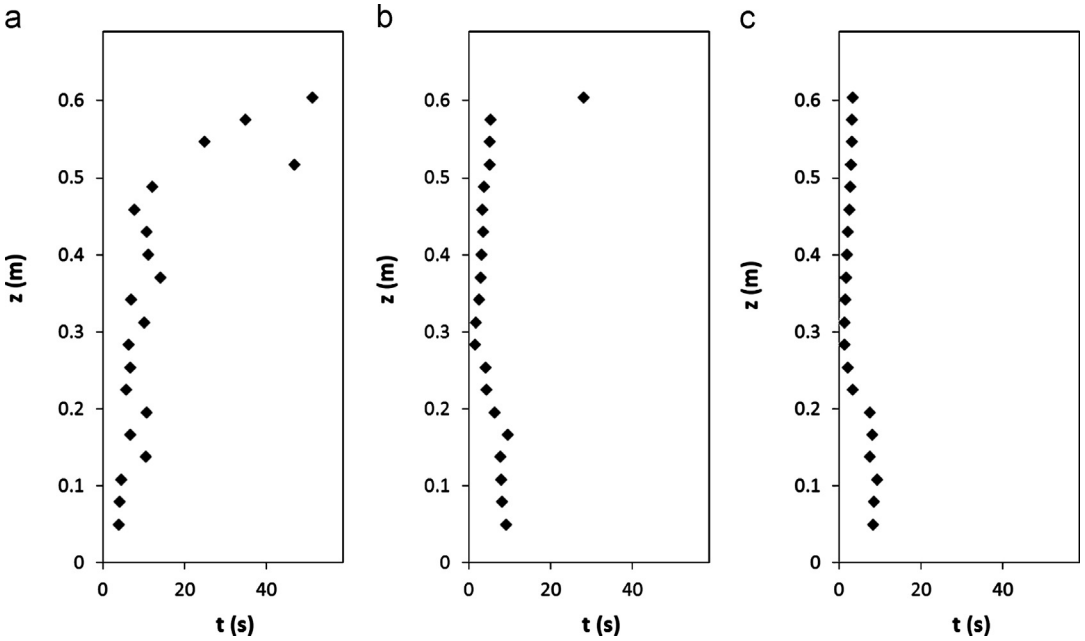

Fig. 8. Mixing times evaluated from injections at different axial positions within the column at representative gas velocities. Liquid: aqueous solution of CMC (1.1% w/w). (a) ug=0021 m/s, (b) ug=0.053 m/s and ug=0.106 m/s.

The mixing times for each gas velocity, calculated from the convergence of the $\Omega(t)$ curves, as indicated in Fig. 7, obtained by reconstructing injections within the region from 10% to 90% of the emulsion expansion, are represented as a function of the gas velocity for the different model liquids in Fig. 9. The mixing times estimated from the reconstructed tracer axial trajectory are in the

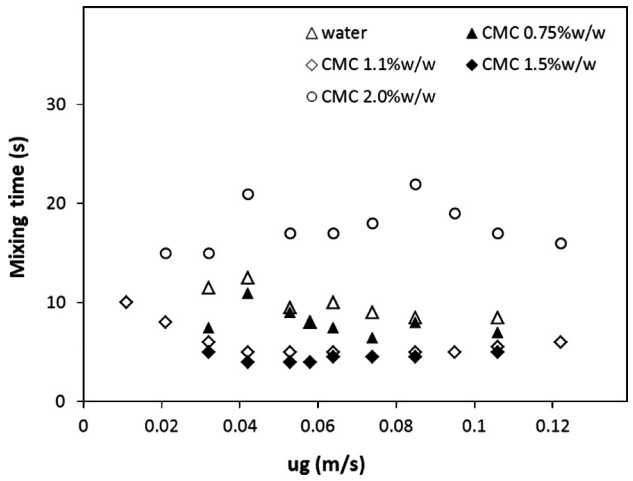

Fig. 9. Influence of the gas velocity and the liquid viscosity on the mixing times calculated from injections at different axial positions within the column.

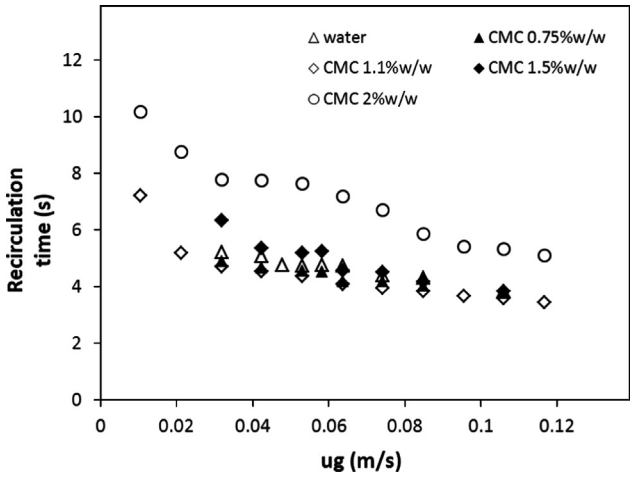

Fig. 10. Influence of the gas velocity and the liquid viscosity on the recirculation times calculated from tracer axial trajectories.

same order of magnitude as those reported in the literature, evaluated from pulse injections of an electrolyte (Rampure et al., 2007; Haque et al., 1987).

There is almost no influence of the gas velocity on the mixing time within the explored range, only a slight negative effect for gas velocities lower than 0.03 m/s. This trend also agrees with those reported in the literature evaluated form conductivity measurements. The influence of liquid viscosity found is not regular. An increase of liquid viscosity initially promotes a decrease of mixing time, particularly arising from the delay induced by injections in the lower part of the column. However, for the highest viscosity liquid, the opposite trend is observed, which could be related to the existence of slug flow in this case, which affects the macroscopic liquid recirculation.

Mixing in bubble columns is ensured locally by dispersion and macroscopically through a gross liquid recirculation imposed by the ascending bubble swarms in the core of the column and descending liquid close to the wall. Faster liquid recirculation leads to shorter times required to attain complete mixing. The gross recirculation can be characterized by only one vortex of the column height as was originally proposed by Hills (1974) or by multiple circulation cells (Joshi et al., 2002; Mudde, 2005). In this case, we have considered only one recirculation cell and determined the recirculation time from the tracer axial trajectory by computing the time between successive crossings of the tracer through the middle of the column in the upwards direction, discarding intervals of less than 0.3 s to avoid fluctuations. Recirculation times calculated from the trajectories for the examined liquids are represented in Fig. 10 as a function of the gas velocity. The influence of gas velocity is initially significant and becomes almost negligible for gas velocities larger than 0.03 m/s, in coincidence with the results found for mixing times. A comparison between Figs. 9 and 10 evidences a link between recirculation and mixing times. Roughly, there is a linear proportionality between mixing and recirculation time. For water and the 0.75% w/w CMC aqueous solution, the proportionality factor is around 2, while it slightly decreases for higher viscosity liquids to around 1.2, except for the highest viscosity solution for which the correlation is less evident probably due to the inception of the slug flow regime.

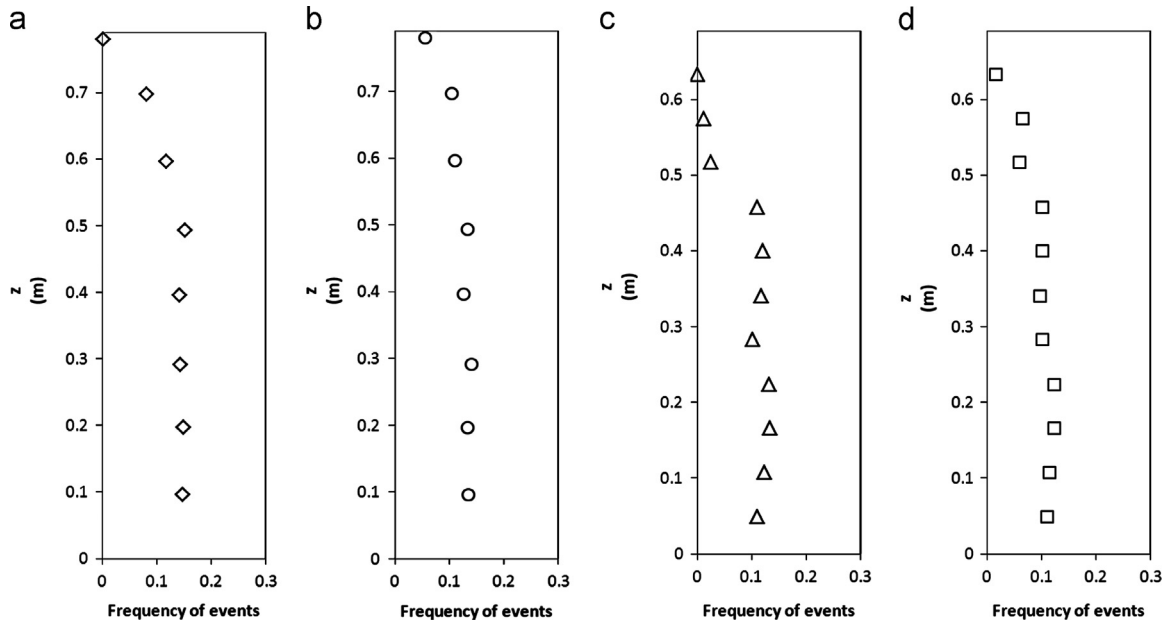

Fig. 11. Frequency of finding the tracer at different axial positions within the column for two model liquids and two gas velocities, as indicated in the legend of the figure. (a) water ug = 0.032 m/s, (b) water ug= 0.106 m/s, (c) CMC 1.1%w/w ug = 0.032 m/s and (d) CMC 1.1%w/w ug = 0.106 m/s.

7. Holdup axial profile

The frequency of finding the tracer at different axial locations in the column is illustrated in Fig. 11 for two examined model liquids and two gas velocities. The frequencies represent the events of the tracer found in a given column volume, referred to the total number of events during the whole tracking period. Frequencies calculated in this way are normalized if the considered regions have different volumes. Since the tracer is neutrally buoyant, it represents the liquid; hence, Fig. 11 would provide an estimation of the liquid holdup axial profile in the column. As observed, the profiles show a moderately decreasing trend along the axial coordinate, reaching zero in the upmost region for low gas velocities, related to the emulsion level in the column. The obtained profiles are neither strongly dependent on the gas velocity nor on the liquid viscosity. It is worthwhile remarking that the frequency of events represents a fraction of liquid holdup, not the local liquid holdup. To recover the actual holdup, the fraction should be multiplied by the number of regions considered and by an average holdup value.

To compare the results with holdup values obtained independently through a different experimental procedure, the gas holdup for given heights along the column were determined using a scanning methodology, locating a gamma emitter opposite to the position of each detector. The gas holdup axial profiles obtained by scanning are shown in Fig. 12 with solid symbols, for the same

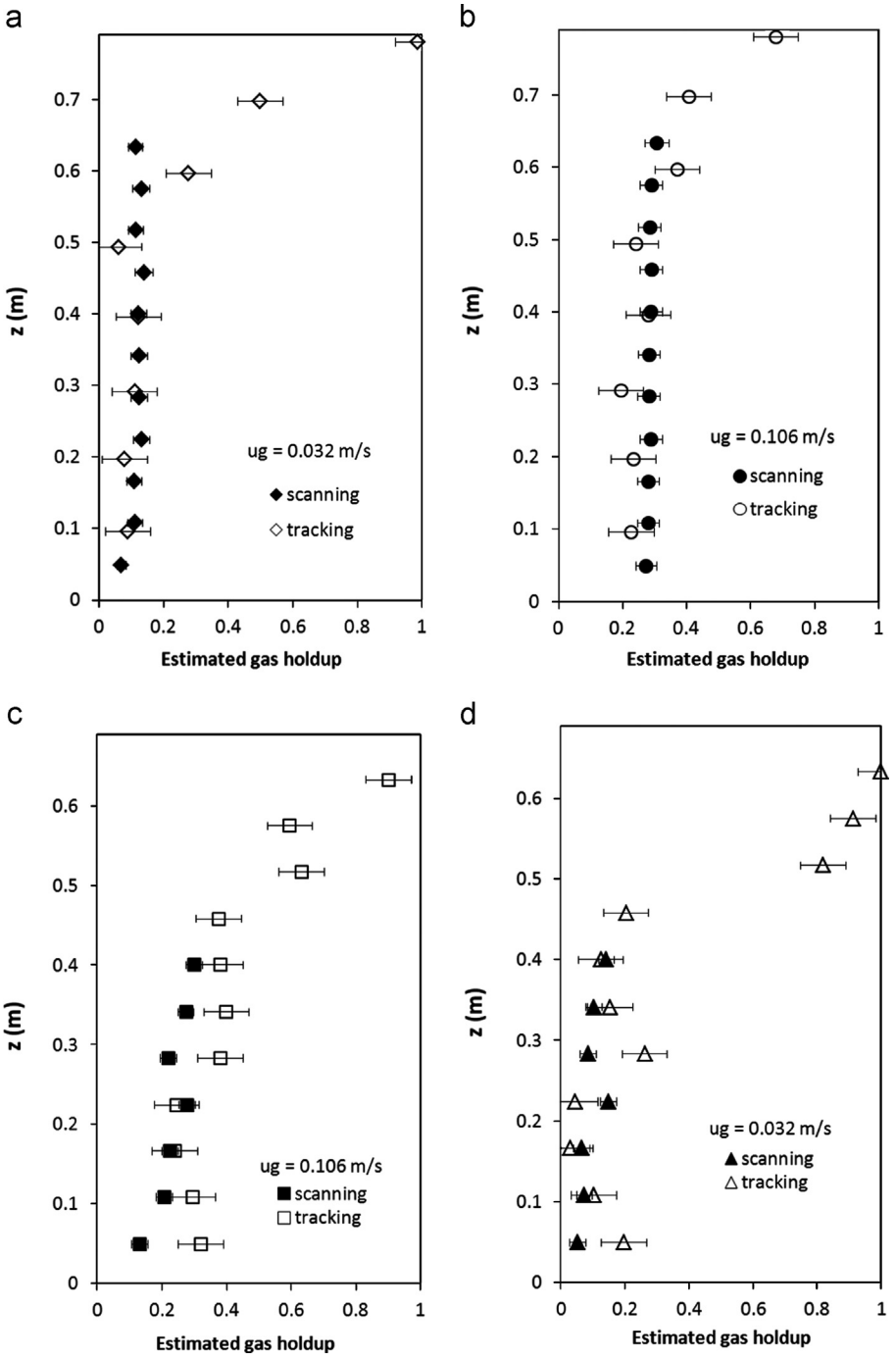

Fig. 12. Comparison of the gas holdup axial profile determined from a standard scanning methodology and estimated from the tracking. (a) water , (b) water, (c) CMC 1.1%w/w and (d) CMC 1.1%w/w.

conditions represented in Fig. 11. The gas holdup estimated from the tracking is shown in the same figure with open symbols for comparison.

Since the frequency of events represents the fraction of liquid holdup distributed in the considered column regions, the liquid holdup is estimated multiplying the frequency of each region by the average liquid holdup determined by scanning and by the number of regions with non-negligible frequencies. Then, the gas holdup is obtained as the difference to 1. The agreement between both experimental estimations of the gas holdup is reasonable, the tracking procedure having larger dispersion than the scanning one. The error of the tracking procedure has been estimated from the mean dispersion of considering the time series divided in 5 portions of 72,000 instants; this leads to a mean statistical variation of around 25% in the fractions of events, which propagates into an error in holdup determination as shown in the figure. The error of the scanning method has been determined as the standard deviation of measuring the chordal holdup six times during 10 s and it is around 10%.

Jin et al. (2005a, b) have provided axial profiles of gas holdup in an industrial scale bubble column and compared holdups determined by the scanning methodology with those obtained through pressure drop measurements. Although the columns size and experimental conditions are totally different, the trend with liquid viscosity of a sharper disengagement for more viscous liquids found by Jin et al. (2005a) is also apparent in the present experiments (compare profiles in Fig. 12a and d).

8. Conclusions

The feasibility of inferring information of the underlying dynamics in bubble columns using a set of axially aligned detectors (AADs) that scan simultaneously different column heights when a unique radioactive tracer is left free within the examined vessel is demonstrated. The combined response of the AADs allows reconstructing the approximate axial trajectory of the tracer along the column.

Distributions of tracer upward and downward fast velocities are determined for different model fluids and gas velocities. The upward tracer velocities increase with the gas velocity and the liquid viscosity. The downward tracer velocities, likely related to the liquid descending velocity while recirculating in the annulus region close to the wall, decrease in absolute value as the liquid viscosity increases and when the gas velocity decreases.

Mixing and recirculation times are also estimated from the tracer axial trajectories for liquids of different viscosities within the range of gas velocities examined. Both mixing and recirculation times slightly depend on gas velocities for low gas velocities and then become almost independent. An increase of liquid viscosity initially promotes axial mixing until very high liquid viscosities for which slug flow is observed leading to a delay in achieving complete mixing.

Liquid holdup axial profiles estimated from the approximate tracer trajectory compares reasonably well with those determined by scanning the column at different heights using an external source.

Acknowledgments

Financial support from CONICET and Universidad de Buenos Aires are gratefully acknowledged. G. Salierno, M. Maestri, M. Cassanello, M. A. Cardona and D. Hojman are members of CONICET. We would particularly like to thank the staff of the RA1 reactor of CNEA, Argentina, for the activation of the sources used in this work.

References

Bhusarapu, S., Cassanello, M.C., Al-Dahhan, M., Dudukovic, M.P., Trujillo, S., O'Hern, T., 2007. Dynamical features of the solid motion in gas–solid risers. Int. J. Multiphase Flow 33, 164–181.

Bird, R.B., Stewart, W.E., Lightfood, E.N., 2006. Transport Phenomena, revised 2nd ed. John Wiley & Sons, Inc..

Cassanello, M., Larachi, F., Guy, C., Chaouki, J., 1996. Solids mixing in gas–liquid–solid fluidization: experiments and modeling. Chem. Eng. Sci. 51, 2011–2020.

Cassanello, M.C., Larachi, F., Kemoun, A., Al-Dahhan, M., Dudukovic, M.P., 2001. Inferring liquid chaotic dynamics in bubble columns using CARPT. Chem. Eng. Sci. 56, 6125–6134.

Chaouki, J., Larachi, F., Dudukovic, M.P. (Eds.), 1997. Elsevier, New York.

Chen, R.C., Reese, J., Fan, L.-S., 1994. Flow structure in a three-dimensional column and three-phase fluidized bubble bed. AIChE J. 40, 1093–1104.

Cover, T.M., Thomas, Y.A., 1991. Elements of Information Theory. Wiley, New York.

Degaleesan, S., Dudukovic, M.P., Pan, Y., 2001. Experimental study of gas-induced liquid-flow structures in bubble columns. AIChE J. 47, 1913–1931.

Devanathan, N., Moslemian, D., Dudukovic, M.P., 1990. Flow mapping in bubble columns using CARPT. Chem. Eng. Sci. 45, 2285–2291.

Dudukovic, M.P., 2002. Opaque multiphase flows: experiments and modeling,. Exp. Therm. Fluid Sci. 26, 747–761.

Fraguío, M.S., 2010. Estudio Fluidodinámico de Reactores Multifásicos Mediante Técnicas de Análisis no-Invasivo. Ph.D. Thesis. Universidad de Buenos Aires. ⟨http://digital.bl.fcen.uba.ar/Download/Tesis/Tesis_4747_Fraguio.pdf⟩.

Groen, J.S., Oldeman, R.G.C., Mudde, R.F., Van Den Akker, H.E.A., 1996. Coherent structures and axial dispersion in bubble column reactors. Chem. Eng. Sci. 51, 2511–2520.

Haque, M.W., Nigam, K.D.P., Srivastava, V.K., Joshi, J.B., Viswanathan, K., 1987. Studies on mixing time in bubble columns with pseudoplastic (carboxymethyl) cellulose solutions. Ind. Eng. Chem. Res. 26, 82–86.

Heindel, T.J.A., 2011. Review of X-ray flow visualization with applications to multiphase flows. J. Fluids Eng. 133, 074001-1–074001-16.

Hills, J.H., 1974. Radial non-uniformity of velocity and voidage in a bubble column. Trans. Inst. Chem. Eng. 52, 1–9.

Joshi, J.B., Vitankar, V.S., Kulkarni, A.A., Dhotre, M.T., Ekambara, K., 2002. Coherent flow structures in bubble column reactors. Chem. Eng. Sci. 57, 3157–3183.

Jin, H., Yang, S., Guo, Z., He, G., Tong, Z., 2005a. The axial distribution of holdups in an industrial-scale bubble column with evaluated pressure using γ-ray attenuation approach. Chem. Eng. J. 115, 45–50.

Jin, H., Yang, S., He, G., Guo, Z., Tong, Z., 2005b. An experimental study of holdups in large-scale p-xylene oxidation reactors using the γ-ray attenuation approach. Chem. Eng. Sci. 60, 5955–5961.

Kantarci, N., Borak, F., Ulgen, K.O., 2005. Review: bubble column reactors. Process Biochem. 40, 2263–2283.

Larachi, F., Cassanello, M., Chaouki, J., Guy, C., 1996. Flow structure of the solids in a three-dimensional gas–liquid–solid fluidized bed. AIChE J. 42, 2439–2452.

Larachi, F., Kennedy, G., Chaouki, J., 1994. A g-ray detection system for 3-D particle tracking in multiphase reactors. Nucl. Instrum. Methods Phys. Res. Sect. A 338, 568–576.

Lee, D.H., Macchi, A., Grace, J.R., Epstein, N., 2001. Fluid maldistribution effects on phase hold ups in three-phase fluidized beds. Chem. Eng. Sci. 56, 6031–6038.

Mudde, R., 2005. Gravity-driven bubbly flows. Annu. Rev. Fluid Mech. 37, 393–423.

Rampure, M.R., Kulkarni, A.A., Ranade, V.V., 2007. Hydrodynamics of bubble column reactors at high gas velocity: experiments and computational fluid dynamics (CFD) simulations. Ind. Eng. Chem. Res. 46, 8431–8447.

Shannon, C.E., 1948. A mathematical theory of communication. Bell Syst. Tech. J. 27, 379–423.

Wilkinson, P.M., Spek, A.P., van Dierendonck, L.L., 1992. Design parameters estimation for scale-up of high pressure bubble columns. AIChE J. 38, 544–554.